Published in final edited form as:
Biomaterials. 2014 September ; 35(27): 7851–7859. doi:10.1016/j.biomaterials.2014.05.088.

In vivo monitoring of structural and mechanical changes of tissue scaffolds by multi-modality imaging

Dae Woo Park[a], **Sang-Ho Ye**[c,d], **Hong Bin Jiang**[c,d], **Debaditya Dutta**[a], **Kazuhiro Nonaka**[c,d], **William R. Wagner**[b,c,d], and **Kang Kim**[a,b,d,*]

Kang Kim: kangkim@upmc.edu

[a]Center for Ultrasound Molecular Imaging and Therapeutics, Department of Medicine, University of Pittsburgh School of Medicine; Heart and Vascular Institute, University of Pittsburgh Medical Center (UPMC), Pittsburgh, PA 15213, USA

[b]Department of Bioengineering, University of Pittsburgh School of Engineering, Pittsburgh, PA 15213, USA

[c]Department of Surgery, University of Pittsburgh School of Medicine, Pittsburgh, PA 15213, USA

[d]McGowan Institute for Regenerative Medicine, University of Pittsburgh and UPMC, Pittsburgh, PA 15219, USA

Abstract

Degradable tissue scaffolds are implanted to serve a mechanical role while healing processes occur and putatively assume the physiological load as the scaffold degrades. Mechanical failure during this period can be unpredictable as monitoring of structural degradation and mechanical strength changes at the implant site is not readily achieved in vivo, and non-invasively. To address this need, a multi-modality approach using ultrasound shear wave imaging (USWI) and photoacoustic imaging (PAI) for both mechanical and structural assessment in vivo was demonstrated with degradable poly(ester urethane)urea (PEUU) and polydioxanone (PDO) scaffolds. The fibrous scaffolds were fabricated with wet electrospinning, dyed with indocyanine green (ICG) for optical contrast in PAI, and implanted in the abdominal wall of 36 rats. The scaffolds were monitored monthly using USWI and PAI and were extracted at 0, 4, 8 and 12 wk for mechanical and histological assessment. The change in shear modulus of the constructs in vivo obtained by USWI correlated with the change in average Young's modulus of the constructs ex vivo obtained by compression measurements. The PEUU and PDO scaffolds exhibited distinctly different degradation rates and average PAI signal intensity. The distribution of PAI signal intensity also corresponded well to the remaining scaffolds as seen in explant histology. This evidence using a small animal abdominal wall repair model demonstrates that multi-modality imaging of USWI and PAI may allow tissue engineers to noninvasively evaluate concurrent

*Corresponding author. Center for Ultrasound Molecular Imaging and Therapeutics, University of Pittsburgh and UPMC, Pittsburgh, PA 15213, USA. Tel.: +1 412 624 5092; fax: +1 412 624 2264.

mechanical stiffness and structural changes of tissue constructs in vivo for a variety of applications.

Keywords

photoacoustic imaging; ultrasound shear wave imaging; elasticity imaging; tissue engineering scaffold; polyurethane; polydioxanone; abdominal wall repair

1. Introduction

Biodegradable polymeric scaffolds have been central to the tissue engineering approach wherein cells infiltrate, proliferate, and elaborate extracellular matrix (ECM) as the scaffold degrades and the newly formed tissue assumes the mechanical role from the degrading scaffold. To design scaffolds which appropriately transfer their mechanical load over time to the ingrowing tissue, temporal analysis is required that verifies the structural and mechanical integrity of remodeling constructs. Current analysis methods are predominantly destructive, requiring animal euthanasia and construct explantation for histological and direct mechanical characterization [1-4]. In addition, different samples are necessarily measured at different times and variance between specimens and animals weakens the analytical power. Ideally, tissue engineers need a system that can non-invasively monitor remodeling in the same specimen over time [5-8]. Non-invasive monitoring that couples structural degradation and mechanical strength changes in tissue constructs would provide an important tool for tissue engineers to evaluate and better design candidate scaffolds.

In our previous studies [7], ultrasound elasticity imaging (UEI) has been applied in vivo to measure the mechanical strength changes of polymeric scaffolds. The polymeric scaffolds were made from three biodegradable elastomers with varying degradation rates and implanted in a rat muscular abdominal wall. Over a 12 wk period the UEI-determined construct stiffness was in good agreement with compressional measurements and histological determinations. However, UEI is limited in that: 1) it requires mechanical compression which limits its applications to areas where clear physical access can be achieved, 2) the measured strain inside the constructs needs to be normalized to the overall strain applied to the body, which provides a source of error, and 3) the measured strain inside the constructs can be sensitive to the stress distribution that depends on the applied force and surrounding anatomy [8].

Ultrasound shear wave imaging (USWI) can be a better alternative for mechanical strength measurements because this technique is based on remote palpation and provides absolute elastic modulus reconstructed from the shear wave speed measurements. USWI has been applied to quantify the shear modulus in tissue by generating transient ultrasound (US) radiation force excitation. The propagation speed of the shear wave is related to the underlying tissue shear modulus [9]. The local tissue shear modulus can be determined in vivo from the displacement field of shear waves using an inversion of the Helmholtz equation [10, 11].

In addition to knowing the temporal mechanical changes occurring spatially at the site of an implanted scaffold, it is desirable to monitor the scaffold degradation process in a coupled fashion. The relative amount of scaffold remaining, whether scaffold degradation is occurring preferentially in one area and whether tissue ingrowth appears to be matching scaffold removal are examples of desired information. However, in vivo assessment of scaffold structural degradation becomes challenging, particularly at the point when fragmentation occurs and these fragments are imbedded within ingrowing tissue. Photoacoustic imaging (PAI) provides a means by which subtle structural changes or small scaffold fragments may be detectable with proper optical contrast. PAI, which combines optical excitation and US detection, has been applied in biomedical applications mostly for the examination of native tissue [12, 13]. In a few studies, photoacoustic microscopy (PAM) techniques have been applied to tissue engineering. The capacity to visualize cell proliferation in a porous polymeric scaffold has been demonstrated in vitro using fibroblasts, embryonic stem cells, and tumor cells [14, 15]. Vascular ingrowth into a tissue engineering construct was displayed in vivo by Cai et al. [16]. However, these PAM approaches have imaging depths only up to a few millimeters [8, 17] and would provide limited information on changes in scaffolds implanted deep in a tissue. To our best knowledge, there have been no reports applying a PAI technique to monitor the structural changes of implanted polymeric scaffolds in vivo.

The objective of this study was to demonstrate the feasibility of combining USWI and PAI in a multi-modality approach to temporally assess the mechanical and structural properties of polymeric scaffolds implanted in a rat abdominal repair model. Two biodegradable polymers with different stiffness and degradation profiles were utilized: poly(ester urethane urea) (PEUU) for a soft material with moderate degradation rate and polydioxanone (PDO) for a stiff material with faster degradation rate. Scaffolds were stained with indocyanine green (ICG) for optical contrast. The mechanical and structural changes determined by non-invasive imaging were compared to explanted samples subjected to direct mechanical and histological analysis.

2. Materials and Methods

2.1. Scaffold Fabrication

PEUU was synthesized based on poly(caprolactone) diol (PCL, Mn=2000, Sigma) and diisocyanatobutane (BDI, Sigma), followed by chain extension with putrescine (Sigma) [18]. PDO was purchased from Sigma-Aldrich (CAS No. 31621-87-1, St. Louis, MO). Wet electrospun PEUU and PDO scaffolds were fabricated by a combination of electrospinning and electrospraying previously reported [19, 20]. Polymer solution from a mounted syringe pump was fed at 1.5 mL/h through a stainless steel capillary (1.2 mm inner diameter) and the capillary was perpendicularly located 15 cm from targeted a stainless steel mandrel (19 mm diameter) rotating at 250 rpm. At the same time, Dulbecco's Phosphate Buffered Saline (DPBS) solution was fed at 12 mL/h through a capillary suspended 5 cm over the mandrel during the electro-spinning. The mandrel was mounted on a stage that reciprocally translated 8 cm along the direction of the mandrel axis at a rate of 0.15 cm/s. Three high-voltage generators were used to charge the polymer feeding capillary to 10 kV, the DPBS feeding

capillary to 8kV and the mandrel (ground) to −4 kV. After 7 h, the fibrous sheet (sample thickness: 0.8-1.0 mm) was removed from the mandrel and stored in DPBS at room temperature overnight. Subsequently, the PEUU and PDO scaffolds were immersed in ICG (PSA1355, H.W. SANDS CORP, FL, USA) solution (0.2g/L in acetone: H_2O = 98:2) for 24 h to achieve ICG staining and washed with DPBS (at least 10 times) to remove unbound ICG). Scaffolds were then stored in DPBS. Square wet electrospun patches of 1 cm by 1 cm were cut and then were sterilized under ultraviolet (UV) irradiation prior to implantation.

Elution of ICG dye from the scaffold was examined in vitro. The scaffolds dyed with ICG were kept in DPBS solution under a continuous rocking condition at 37°C. The concentrations of ICG in the solution were measured at 1, 2, 4, 8 and 12 weeks using an UV spectrum with an 800 nm absorption peak. The remained ICG amounts in the scaffolds were measured after the ICG dye was extracted using a 70% ethyl alcohol solution.

2.2. Animal Preparation

Female Lewis 12-week old rats (200 g) were used under a protocol consistent with the National Institutes of Health (NIH) guidelines for animal care and approved by the University of Pittsburgh Institutional Animal Care and Use Committee. The surgery was performed in a sterile environment using a procedure based on a previous study [7]. An incision was made along the midline of the abdomen, and subcutaneous pockets were created in each side of the abdominal wall. A full thickness square defect (1×1 cm) involving all layers of the abdominal wall, including external oblique, internal oblique and transverse abdominis muscle and peritoneum was created in each pocket. Two same type of scaffold were implanted for each rat. Total of 36 rats were evenly divided into two groups where 18 rats were implanted with PEUU and 18 with PDO. The rats were sacrificed in four batches; at week 0 (n=3 for each group), at week 4 (n=5 for each group), week 8 (n=4 for PEUU and n=5 for PDO group), and week 12 (n=5 for each group). Note that there is one less rat at week 8 for PEUU group due to unexpected death for unknown reason between week 4 and 8. After sacrifice, all scaffolds were harvested, for either compression testing or histological assessments as summarized in Table 1.

2.3. Ultrasound Shear Wave Imaging

The experimental setup for USWI is shown in Fig. 1. USWI pulse/imaging sequences were implemented on a commercial US scanner (US scanner I) (V-l, Verasonics Inc., Redmond, WA, USA) connected with a clinical transducer (L7-4, ATL 5 MHz central frequency). Using 128 transducer elements, four push pulses of 180 μs long were sequentially induced at four depths 23.7, 28.6, 33.6 and 38.5 mm (white dots in Figs. 2A and 2B) to create a planar shear wave. Immediately after, a very high frame rate imaging of 8000 Hz was performed by transmitting unfocused plane-waves with 64 transducer elements of the probe to record the propagating shear wave [11]. All backscattered radio frequency (RF) frames were stored in each channel of 64, then transferred to a computer.

In vitro USWI was performed using a scaffold embedded in a tissue mimicking phantom block. A piece of wet PEUU scaffold (1 × 1 × 0.6 cm) was placed 1 cm below the surface of a plastic container (15 × 10 × 6 cm) filled with 10% PVA solution (Fig. 2A), mixed with US

scatterers, cellulose powder 5% by weight of the PVA solution (Sigmacell, 20μ, Sigma-Aldrich, St. Louis, MO). After two cycles of freezing at -20 °C for 12 h and thawing in room temperature for 12 hours, the container was removed from the phantom block. The phantom block was placed in a water tank and localized US push pulses were generated by a Philips L7-4 clinical transducer. The same transducer then subsequently acquired RF frames during 4 ms while the created shear wave was propagating through the phantom block. Axial displacements of the shear wave were calculated from the RF frames using the Loupas' algorithm, 1-D autocorrelation function [21, 22]. The axial displacements at the focal depth of the push pulses were averaged over 10 frames to improve the signal-to-noise ratio (SNR). Finally, the shear modulus was then determined from the axial displacements field using an inversion of the Helmholtz equation (Fig. 2B) [10, 11].

For in vivo USWI, rats were anesthetized in supine position on a heated platform with the abdomen exposed to the US transducer, as depicted in Fig. 1. The US scan was performed on a monthly basis from the first scan day until the animal was euthanized. The shear modulus of PEUU and PDO scaffolds and neighboring native abdominal wall tissues were measured at week 0, 4, 8 and 12.

2.4. Photoacoustic Imaging

The experimental setup for PAI is displayed in Fig.1. Q-switched Nd:YAG pulsed Laser (Quantel, Bozeman, MT, USA) pumps an optical parametric oscillator (OPO) (Vibrant HE532I, OpoTek, Carlsbad, CA, USA) to generate 5 ns pulses at 10 Hz. The laser beam of OPO output was illuminated through the optic fiber bundle on the target. Light fluence on the animal skin was measured 5 mJ/cm^2 for both at 750 nm and 800 nm, which is below the ANSI safety limit (20 mJ/cm2) [23]. The laser beam area was measured 30 mm × 20 mm, which is large enough to uniformly illuminate the entire area of the scaffolds. A linear array transducer (L14-5, 6 MHz) connected to a commercial US scanner (US scanner II) (SonixTouch, Ultrasonix Corp., Canada) was used to receive the PAI signal and B-mode images.

In vivo PAI was performed followed by USWI on the same animal prepared following the same procedure described in section 2.3. To remove PAI signal from the animal skin and background tissues, a two wavelength subtraction method (750 nm and 800 nm) was applied [24]. The ICG has a distinct absorption peak at about 800 nm from 750 nm [25], while changes in the absorption of melanin in skin are negligible in this range of wavelengths [26]. The PAI signal intensity was spatially averaged over the entire region of each construct and the mean value was taken over 10 samples. A two tailed t-test was performed for the mean PAI signal intensity of PEUU and PDO constructs.

In-vitro PAI was performed using ICG dyed PEUU and PDO scaffolds embedded in a PVA phantom block. The PVA phantom block was fabricated following the same procedure described in section 2.3. The scaffolds were embedded 2 cm below the top surface of the phantom block. The phantom block was placed in a water tank and was illuminated by the laser pulses at wave length 800 nm. The PAI signal intensity was averaged 3 times at each scan to minimize the pulse-to-pulse energy variation and increase SNR. The PAI signal

intensity was normalized to the measured average pulse energy (J-50MB-YAG Energy Max™ Sensor, Coherent, Portland, OR).

2.5. Direct Mechanical Measurement (Compression Test)

The compression test was performed using an electromechanical testing machine (Insight, MTS Systems, Eden Prairie, MN, USA) following the same procedure as previous study [7]. The Young's modulus was calculated at the first 10% strain from the slope of the stress-strain curves. For PEUU scaffolds, six samples (6 constructs) were evaluated at week 0, four samples were evaluated at week 8 and five samples each were evaluated at week 4 and 12. For PDO scaffolds, six samples (6 constructs) were evaluated at week 0, five samples each were evaluated at week 4, 8 and 12 (see Table 1). Using an additional group of 12 animals, the native abdominal wall samples of 6 from 3 animals were evaluated at each week of 0, 4, 16 and 24.

2.6. Histology & Collagen Deposition Measurement

The Masson's trichrome (MT) staining for histological analysis was performed following the same procedure as previously reported [7]. The constructs were fixed in 10% formalin solution for 24 h right after the sacrifice, sectioned and stained with MT. For PEUU, five samples each (5 constructs) were prepared at weeks 4 and 12 and four samples were prepared at week 8. For PDO, five samples each were prepared at weeks 4, 8 and 12 (see Table 1). Magnified images were taken from representative standard regions within the samples. The average percentage of collagen area was calculated for each magnified image using the same procedure as previously reported [7]. The average percentage of collagen area in the total area was measured by ImageJ (National Institutes of Health, Bethesda, MD, USA). The one-way analysis of variance (ANOVA) was performed for the average percentage of collagen area of PEUU and PDO constructs at weeks 4, 8 and 12.

3. Results

USWI and PAI were performed in vitro on PEUU scaffolds dyed with ICG and embedded in a tissue mimicking phantom block made of polyvinyl alcohol (PVA, Sigma-Aldrich, St. Louis, MO). Fig. 2A illustrates the propagation of the shear wave laterally (across the US beam direction) in a PVA phantom block containing a PEUU scaffold. Red color represents axial (along the US beam direction) displacements away from the transducer and these axial displacement maps were captured at 0.6, 1.3, 1.8 and 2.4 ms after generating US push pulses at four depths marked by white dots in Figs. 2A and 2B. The embedded PEUU scaffold is identified by white dashed circles. It is noted that the shear wave front (red) advances as soon as it propagates into the scaffold area, reflecting an increase of the shear wave speed. Fig. 2B presents a shear modulus map calculated from the displacement field of shear waves using an inversion of the Helmholtz equation. The larger shear modulus estimated within the scaffold clearly indicates that the embedded scaffold is stiffer than the surrounding PVA phantom block. In Fig. 2C under visible light three scaffolds are seen embedded in a PVA phantom block: a 1cm long undyed PEUU scaffold, and a 1 cm and a 1 mm long PEUU scaffold dyed with ICG. PAI signal intensity from the embedded scaffolds laid over a B-mode image is displayed in Fig. 2D. The high PAI signal intensity clearly identifies the ICG

dyed scaffolds of 1 cm long and 1 mm long from the background and the neighboring undyed scaffold, being co-registered well with the B-mode image (Fig. 2D) and the picture (Fig. 2C). To optimize the contrast in color, the dynamic range of PAI signal intensity was set to 20 dB. Similarly sized PDO scaffolds dyed with ICG were also well identified by PAI under the same conditions (data not presented).

The USWI and PAI were then applied in vivo to longitudinally monitor both the stiffness and structural changes of implanted scaffolds. In addition, the UEI was also applied, following the same protocol as described previously, using the same ultrasound scanner (US scanner III) (Vevo2100, Visualsonics, Canada) [7]. Table 1 summarizes the animal groups, scans of USWI, PAI, and UEI and number of the constructs for mechanical testing and histology at each time point. Fig. 3 provides typical reconstructed shear modulus maps of PEUU or PDO constructs in the rat abdominal wall and overlaid B-mode images over the implant period. The scaffold and neighboring native abdominal wall areas of interest are denoted as white and red dashed circles, respectively. Most of the stiffness changes for both the PEUU and PDO scaffolds were observed between week 0 and 8. During this period, the stiffness of PEUU first increased and then started decreasing at week 4, while PDO continued to become softer up to week 8.

Fig. 4A displays the Young's modulus of the explanted constructs obtained by compression testing at weeks 0, 4, 8, and 12. In a separate additional group of 12 animals, the Young's modulus of the native abdominal wall remained constant around 3.9±0.2 kPa up to 20 weeks. Fig. 4B presents the average shear modulus obtained by USWI of the constructs (red open triangle) and the adjacent, non-implanted tissue (blue open square) over time. The shear modulus in each construct within the white dashed circle and neighboring native abdominal wall area on the opposite side within the red dashed circle depicted in Fig. 3 was spatially averaged, and then, the mean value was taken over 10 samples. It is noted that the stiffness of PEUU scaffolds approximated that of the native surrounding tissues after 8-12 weeks of implantation. On the other hand, the stiffness of PDO scaffolds decreased continually and became slightly below the neighboring native abdominal wall tissues after week 8. Scatter plots indicating the correlation of the Young's modulus obtained by compression test and shear modulus obtained by USWI from the same samples at the corresponding time points are shown in Fig. 4C.

In Fig. 5, histology is presented with MT stained images for PEUU and PDO scaffolds at weeks 4, 8 and 12. Areas with cellular infiltration contrast to the white areas of scaffold regions without infiltration. In Fig. 5C, the collagen deposition was quantified by assuming blue staining in the Fig. 5B images represented collagen. The collagen deposition was high at week 4 and gradually decreased through week 12 ($P<0.05$) for PEUU group. For PDO group, the overall collagen deposition changes from week 4 to week 12 were not significant ($P>0.05$).

In Fig. 6, the PAI signal intensity maps for PEUU and PDO scaffolds, respectively, in the rat abdomen at weeks 4, 8 and 12 are seen. For presentation purposes, the dynamic range of the color maps was set to 20 dB. Figs. 6B and 6F present MT staining of PEUU and PDO constructs, respectively, at weeks 4, 8 and 12. In Figs. 6C and 6G, magnified images from

representative central areas in the scaffolds, where minimal cellular infiltration occurred, are displayed. In Figs. 6D and 6H, magnified images of representative areas in the peripheral region of the PEUU and PDO scaffolds are seen. Substantial cellular ingrowth (red) and collagen elaboration (blue) was observed for both scaffolds.

PAI intensity maps overlaid on B-mode images are depicted in Fig. 7A for a rat implanted with a scaffold made from PEUU (top panels) and PDO (bottom panels), and continually monitored at week 0, 4, 8 and 12. The areas with high PAI signal intensity correspond with scaffold regions experiencing minimal cellular infiltration. Fig. 7B shows the average of PAI signal intensity of PEUU and PDO constructs at each time point. The PAI signal intensity was spatially averaged over the entire region of each construct as shown in Fig. 7A, and then, the mean value was taken over 10 samples. The background PA signal intensity in Fig. 7B was obtained from the region neighboring the implantation site to provide baseline PAI signal intensity for tissues without scaffolds. The average PAI signal intensity was similar between PEUU (-25.4±2.8 dB) and PDO (-26.3±2.9 dB) at the time of implantation. The PAI signal intensity from PEUU gradually decreased from week 0 to week 12, while the PAI signal intensity from PDO sharply decreased from week 0 to week 8 the decrease was minimal from week 8 to 12.

4. Discussion

Distinct differences in stiffness change over time between soft PEUU scaffolds with a moderate degradation rate and stiff PDO scaffolds with a faster degradation rate were imaged and analyzed. At week 0, PEUU was more compliant than PDO as shown in USWI results and compression tests (Fig. 4). At week 4, the average shear modulus of PEUU reached the peak value above the shear modulus of neighboring native abdominal wall tissues, then it continued to decrease through week 8 and became close to the value of the neighboring native abdominal wall tissues after being implanted for 12 weeks. On the other hand, the average shear modulus of PDO constructs decreased monotonically for 8 weeks and reached a plateau at or slightly lower than that of the neighboring native abdominal wall tissues. Based on the compression tests, the Young's modulus of the native abdominal wall remained unchanged. In general, a risk for a scaffold that degrades too rapidly is that the ingrowing tissue is not adequate in quantity or structure to assume the mechanical properties characteristic of nearby tissue, or to fulfill the mechanical role of the replaced tissue. For the PDO scaffold, the mechanical properties deteriorated relatively quickly to a point where the reconstructed site was eventually equal to or lower than the host tissue. It is possible that at later time points this site could further weaken if the ingrowing tissue did not adequately develop based on a too rapidly degrading scaffold. The histological determination of collagen area was reasonably in good agreement with the overall stiffness change of the constructs reflected by USWI for PEUU scaffolds. However, for PDO scaffolds that degraded and thinned out rapidly over 12 weeks, the change in percent area of collagen deposition may not well represent the stiffness change of constructs. Although the underlying specific biological processes such as interplay of cells and extracellular matrix were not investigated here, as show in Fig. 4, a consistent trend in overall mechanical strength change among the same type of samples was observed. For both PEUU and PDO, the shear modulus changes between each time point (presented in Fig. 4.) as measured by

USWI were significant ($p<0.05$). The smallest change in shear modulus was about 0.5 kPa. The Young's modui of PEUU and PDO scaffolds measured by compression testing were 6 kPa and 12 kPa, respectively at week 0 (Fig. 4). It is expected that the USWI can be used for harder scaffolds with limitations due to attenuation of ultrasound and shear wave. For native tissue imaging, the USWI has been applied to contracted muscle with Young's modulus of 270 kPa [27].

One of limitations in relating the mechanical parameters obtained from ultrasound imaging and ex vivo evaluation is that a shear modulus is determined from USWI and the Young's modulus from the compression tests (Fig. 4). For soft tissues, the Young's modulus and shear modulus are related with a constant of the Poisson ratio, ν, which is close to 0.5. The Young's modulus E can be considered to be approximately three times the shear modulus, μ ($E \approx 3\mu$) [11]. However, the Poisson's ratio of the implanted constructs may have varied during the scaffold degradation process and with tissue ingrowth, although with no dramatic change in Poisson's ratio was anticipated. Notwithstanding this limitation, the trend of changes over time in the average shear modulus of both constructs obtained by in vivo USWI compared well with the Young's modulus obtained by ex vivo compression tests. Further investigation on detailed mechanical and structural characteristics, including porosity changes and tissue boundary conditions, could be considered to better define this relationship.

UEI was also performed on both PEUU and PDO scaffolds and the results were compared with USWI and our previous UEI study [7] as summarized in Table 1. The change in stiffness (normalized strain) of PEUU and PDO constructs by the UEI correlated well with the stiffness (Young's modulus) by compression tests ($R = 0.8$ and $P<0.05$). The overall stiffness changes in PEUU scaffolds by UEI over time were also consistent with our previous report [7]. Some of the limitations with UEI, where the developed strain can be subject to the applied loading, can be overcome using USWI, which is advantageous for further translation into clinical application. There are, however, some limitations of USWI to be overcome before such translation. While the viscoelastic behavior is expected given the porous structure of the scaffolds, with USWI, only the purely elastic properties can be measured. In this study, based on the Voigt model, only shear storage modulus was reconstructed by using an inversion of the Helmholtz equation and shear loss modulus was not considered [28].

The PAI signal intensity closely agreed with the histologically observed remaining scaffold in explanted tissue sections. The data in Fig. 6 suggest PAI can identify structural changes as they develop in the scaffolds. The ICG dye employed to create optical absorption of the scaffolds in the near infrared range for PAI is approved by the US Food and Drug Administration [29] and has been used for clinical applications including angiography and surgical applications [30]. Recently, a polyurethane sheet containing ICG has been prepared and antimicrobial activity against Gram-positive bacteria under laser light exposure was reported [31]. In terms of the overall degradation process, no observable difference was observed in this study using PEUU scaffolds dyed with ICG relative to the previous study using bare PEUU scaffolds [32]. However, further detailed investigation might be needed to evaluate the effects of ICG on tissue regeneration and repair. In a separate test, ICG-dyed

scaffolds were submerged in phosphate buffered saline, and the accumulated eluting amounts of ICG from the scaffolds were measured. The total accumulated ICG eluted from the scaffold during a three month period was 10.4 (±1.9)% (n = 3), although most of the elution (5 to 7%) was observed at the initial time points (1 and 2 weeks) and after that the elution was minimal. This suggests that the measured loss in the PAI signal is mostly related to clearance of ICG together with the polymer as scaffold degradation ensues.

The imaging depth for PAI is limited by light diffusion from tissue scattering [17]. The imaging depth for USWI is limited by attenuation of acoustic radiation force [9]. For both USWI and PAI at near infrared, the typical imaging depth is up to 5 cm [9-11, 17]. Both techniques could be applied to engineered tissues or organs within 5 cm of a probe, such as for vascular grafts, bladder, and kidney [33-35].

In future studies, we will combine the USWI and PAI techniques into a single platform system to obtain an automatically co-registered structural PAI image and mechanical USWI image. The use of this combined system for real-time in-vivo animal studies will significantly reduce the variability of measurements between animals, and consequently shorten the study period. Such a technology could be utilized as a clinical tool to monitor the development of tissue engineering treatments.

5. Conclusions

The change in shear modulus of the constructs obtained by USWI for both PEUU and PDO scaffolds in vivo compared well with the change in Young's modulus of the constructs obtained by ex vivo compression tests. The PAI signal intensity map closely agreed with histological determination of the remaining scaffold area in explanted samples at corresponding time points for both PEUU and PDO constructs. The different degradation rates between PEUU and PDO constructs were well reflected both in average PAI signal intensity and in average shear modulus over time. The reported findings and observations in this study using a small animal abdominal wall repair model demonstrate that a non-invasive multi-modality approach using USWI and PAI may allow tissue engineers to sequentially evaluate the remodeling of tissue scaffolds both in terms of mechanics and structural changes in vivo for diverse applications.

Acknowledgments

The authors would like to thank Ms. Linda Lavery for the animal preparation; Dr. Choon Hwai Yap for helpful discussions; Dr. Kee-Won Lee and Dr. Yadong Wang for use of instrumentation and help for compression tests. This work was supported by NIH R21 EB013353. Small animal imaging scanner –Vevo2100 was supported with an NIH shared instrument grant (1S10RR027383).

References

1. Martinez-Diaz S, Garcia-Giralt N, Lebourg M, Gomez-Tejedor JA, Vila G, Caceres E, et al. In vivo evaluation of 3-dimensional polycaprolactone scaffolds for cartilage repair in rabbits. Am J Sports Med. 2010; 38:509–19. [PubMed: 20093424]
2. Yoshikawa M, Yabuuchi T, Tsuji N, Shimomura Y, Hayashi H, Ohgushi H. In vivo osteogenesis in porous hydroxyapatite scaffold processed in hyaluronic acid solution. Key Eng Mater. 2008:361–363. 1185–8.

3. VandeVord PJ, Matthew HWT, DeSilva SP, Mayton L, Wu B, Wooley PH. Evaluation of the biocompatibility of a chitosan scaffold in mice. J Biomed Mater Res. 2002; 59:585–90. [PubMed: 11774317]

4. Lee WK, Ichi T, Ooya T, Yamamoto T, Katoh M, Yui N. Novel poly(ethylene glycol) scaffolds crosslinked by hydrolyzable polyrotaxane for cartilage tissue engineering. J Biomed Mater Res. 2002; 67A:1087–92.

5. Kim K, Jeong CG, Hollister SJ. Non-invasive monitoring of tissue scaffold degradation using ultrasound elasticity imaging. Acta Biomater. 2008; 4:783–90. [PubMed: 18348913]

6. Cohn NA, Kim BS, Erkamp RQ, Mooney DJ, Emelianov SY, Skovoroda AR, et al. High-resolution elasticity imaging for tissue engineering. IEEE T Ultrason Ferr. 2000; 47:956–66.

7. Yu J, Takanari K, Hong Y, Lee KW, Amoroso NJ, Wang Y, et al. Non-invasive characterization of polyurethane-based tissue constructs in a rat abdominal repair model using frequency ultrasound elasticity imaging. Biomaterials. 2013; 34(11):2701–2709. [PubMed: 23347836]

8. Appel AA, Anastasio MA, Larson JC, Brey EM. Imaging challenges in biomaterials and tissue engineering. Biomaterials. 2013; 34:6615–6630. [PubMed: 23768903]

9. Sarvazyan AP, Rudenko OV, Swanson SD, Fowlkes JB, Emelianov SY. Shear wave elasticity imaging: a new ultrasonic technology of medical diagnostics. Ultrasound Med Biol. 1998; 24(9): 1419–1435. [PubMed: 10385964]

10. Nightingale K, McAleavey S, Trahey G. Shear wave generation using acoustic radiation force: in vivo and ex vivo results. Ultrasound Med Biol. 2003; 29:1715–1723. [PubMed: 14698339]

11. Bercoff J, Tanter M, Fink M. Supersonic shear imaging: a new technique for soft tissue elasticity mapping. IEEE Trans Ultrason Ferroelectr Freq Contr. 2004; 51(4):396–409.

12. Xu M, Wang LV. Photoacoustic imaging in biomedicine. Review of Scientific Instruments. 2006; 77(4):041101–041101. 22.

13. Li C, Wang LV. Photoacoustic tomography and sensing in biomedicine. Phys Med Biol. 2009; 54(19):R59–97. [PubMed: 19724102]

14. Zhang Y, Cai X, Choi SW, Kim C, Wang LV, Xia Y. Chronic label-free volumetric photoacoustic microscopy of melanoma cells in three-dimensional porous scaffolds. Biomaterials. 2010; 31:8651. [PubMed: 20727581]

15. Zhang Y, Cai X, Wang Y, Zhang C, Li L, Choi SW, et al. Noninvasive photoacoustic microscopy of living cells in two and three dimensions through enhancement by a metabolite dye. Angew Chem Int Ed. 2011; 123:7497.

16. Cai X, Zhang Y, Li L, Choi SW, MacEwan MR, Yao J, et al. Investigation of neovascularization in three-dimensional porous scaffolds in vivo by a combination of multiscale photoacoustic microscopy and optical coherence tomography. Tissue Engineering: Part C. 2013; 19(3):196–204.

17. Wang LV. Multiscale photoacoustic microscopy and computed tomography. Nature Photonics. 2009; 3:503–509. [PubMed: 20161535]

18. Guan J, Sacks MS, Beckman EJ, Wagner WR. Synthesis, characterization, and cytocompatibility of elastomeric, biodegradable poly(ester-urethane)ureas based on poly(caprolactone) and putrescine. J Biomed Mater Res. 2002; 61:493–503. [PubMed: 12115475]

19. Stankus JJ, Soletti L, Fujimoto K, Hong Y, Vorp DA, Wagner WR. Fabrication of cell microintegrated blood vessel constructs through electrohydrodynamic atomization. Biomaterials. 2007; 28:2738–2746. [PubMed: 17337048]

20. Hashizume R, Fujimoto KL, Hong Y, Amoroso NJ, Tobita K, Miki T, et al. Morphological and mechanical characteristics of the reconstructed rat abdominal wall following use of a wet electrospun biodegradable polyurethane elastomer scaffold. Biomaterials. 2010; 31:3253–3265. [PubMed: 20138661]

21. Loupas T, Peterson RB, Gill RW. Experimental evaluation of velocity and power estimation for ultrasound blood flow imaging, by means of a two-dimensional autocorrelation approach. IEEE Trans Ultra Ferro Freq Contr. 1995; 42(4):689–699.

22. Pinton GF, Dahl JJ, Trahey GE. Rapid tracking of small displacements with ultrasound. IEEE Trans Ultra Ferro Freq Contr. 2006; 53(6):1103–1117.

23. Laser Institute of America. American National Standard for Safe Use of Lasers. ANSI Z136.1-2000. 2000

24. Razansky D, Vinegoni C, Ntziachristos V. Multispectral photoacoustic imaging of fluorochromes in small animals. Optics Letters. 2007; 32(19):2891–2893. [PubMed: 17909608]
25. Landsman MLJ, Kwant G, Mook GA, Zijlstra WG. Light-absorbing properties, stability, and spectral stabilization of indocyanine green. J Appl Physiol. 1976; 40(4):575–583. [PubMed: 776922]
26. Bassukas I, Galaris D, Tsolakidis A, Zonios G, Dimou A, Kaxiras E. Melanin absorption spectroscopy: new method for noninvasive skin investigation and melanoma detection. J Biomed Optics. 2008; 13(1):014017.
27. Shinohara M, Sabra K, Gennisson JL, Fink M, Tanter M. Real-time visualization of muscle stiffness distribution with ultrasound shear wave imaging during muscle contraction. Muscle&Nerve. 2010; 42(3):438–441. [PubMed: 20665510]
28. Deffieux T, Montaldo G, Tanter M, Fink M. Shear wave spectroscopy for in vivo quantification of human soft tissues visco-elasticity. IEEE Transactions on Medical Imaging. 2009; 28(3):313–322. [PubMed: 19244004]
29. Kim C, Song KH, Gao F, Wang LV. Sentinel lymph nodes and lymphatic vessels: noninvasive dual-modality in vivo mapping by using indocyanine green in rats—volumetric spectroscopic photoacoustic imaging and planar fluorescence imaging. Radiology. 2010; 255(2):442–450. [PubMed: 20413757]
30. Alander JT, Kaartinen I, Laakso A, Pätilä T, Spillmann T, Tuchin VV, et al. A review of indocyanine green fluorescent imaging in surgery. Int J Biomed Imaging. 2012; 940585:1–26.
31. Perni S, Pratten J, Wilson M, Piccirillo C, Parkin IP, Prokopovich P. Antimicrobial properties of light-activated polyurethane containing indocyanine green. J Biomater Appl. 2011; 25:387–400. [PubMed: 20008087]
32. Hong Y, Huber A, Takanari K, Amoroso NJ, Hashizume R, Badylak SF, et al. Mechanical properties and in vivo behavior of a biodegradable synthetic polymer microfiber-extracellular matrix hydrogel biohybrid scaffold. Biomaterials. 2011; 32:3387–3394. [PubMed: 21303718]
33. Wu W, Allen RA, Wang Y. Fast-degrading elastomer enables rapid remodeling of a cell-free synthetic graft into a neoartery. Nature Medicine. 2012; 18:1148–1153.
34. Engelhardt EM, Micol LA, Houis S, Wurm FM, Hilborn J, Hubbell JA, Frey P. A collagen-poly(lactic acid-co-ε-caprolactone) hybrid scaffold for bladder tissue regeneration. Biomaterials. 2011; 32(16):3969–3976. [PubMed: 21377203]
35. Sullivan DC, Mirmalek-Sani SH, Deegan DB, Baptista PM, Aboushwareb T, Atala A, Yoo JJ. Decellularization methods of porcine kidneys for whole organ engineering using a high-throughput system. Biomaterials. 2012; 33(31):7756–7764. [PubMed: 22841923]

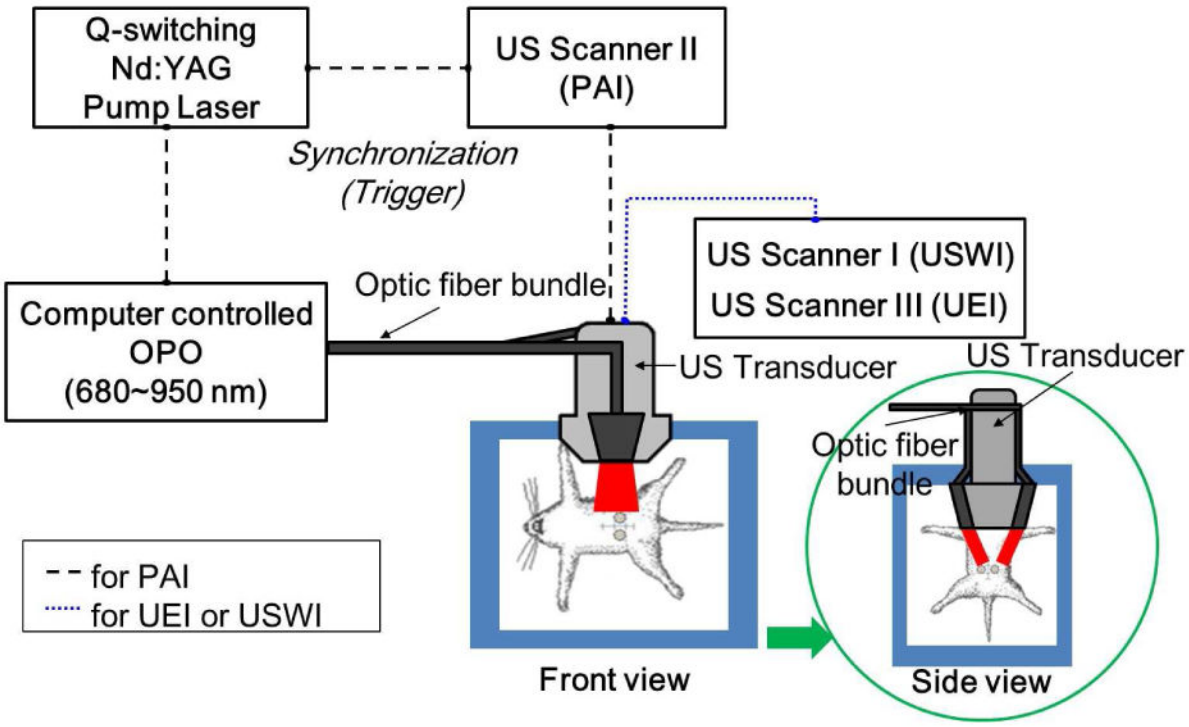

Fig. 1.

Experimental setup for PAI, USWI and UEI. A Nd:Yag pulsed laser pumps an optical parametric oscillator (OPO) to generate 5 ns pulses at 10 Hz. The OPO output laser beam is directed to the optic fiber and illuminates the constructs area (approximately 5 mJ/cm2 of fluence for both 750 and 800 nm). A linear array transducer (L14-5, 6 MHz) connected to a commercial US scanner was used to receive the PAI signal and B-mode images. For USWI and UEI, the laser system was not used.

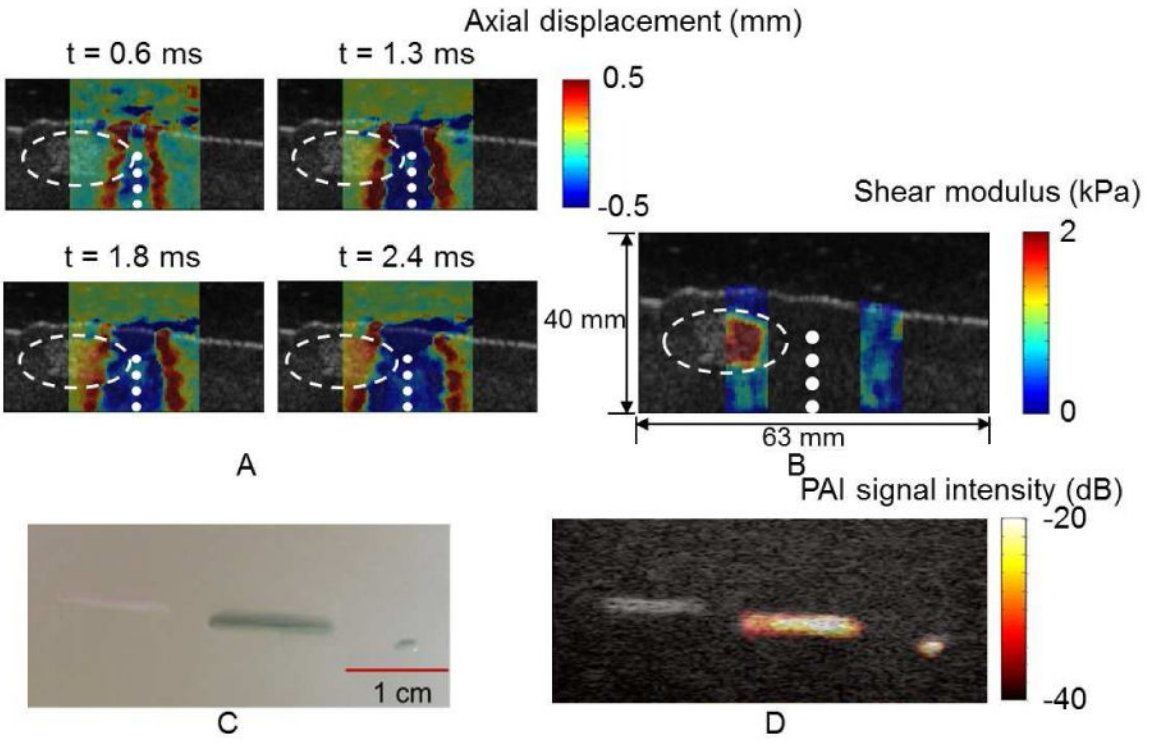

Fig. 2.

In vitro USWI and PAI on PEUU dyed with indocyanine green (ICG) embedded in a polyvinyl alcohol (PVA) phantom block. (A) Shear wave propagation in the lateral direction (across the ultrasound beam direction) is seen. Color represents axial (along the ultrasound beam direction) displacements in a PVA phantom block containing a PEUU scaffold identified by the dashed circles. The locations of applied ultrasound pushing pulses are marked white dots. (B) A shear modulus map calculated from the axial displacement field using an inversion of the Helmholtz equation. (C) Three PEUU scaffolds seen in visible light, left to right, a 1 cm undyed scaffold, and 1 cm and 1 mm scaffolds dyed with ICG. (D) Corresponding PAI signal intensity laid over a B-mode image.

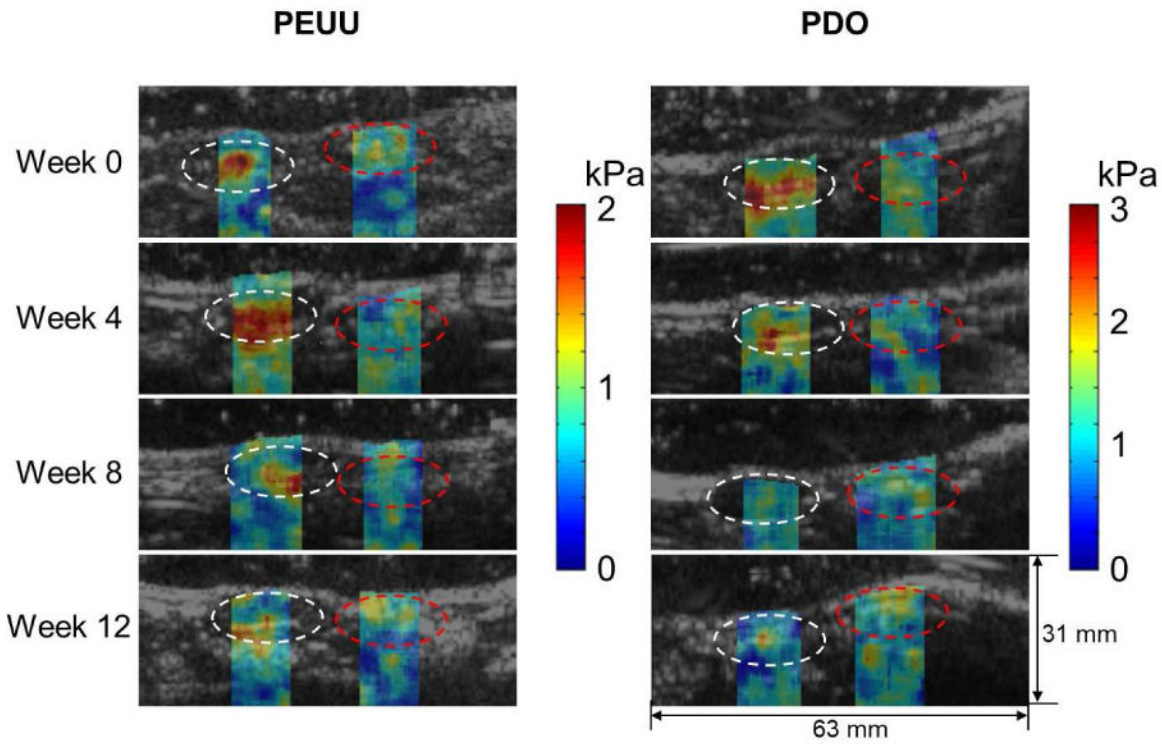

Fig. 3.

Typical reconstructed shear modulus maps of the PEUU and PDO scaffolds implanted in the rat abdominal wall and overlaid B-mode images over time. The scaffold and neighboring native abdominal wall tissue areas of interest are denoted as white and red dashed circles, respectively.

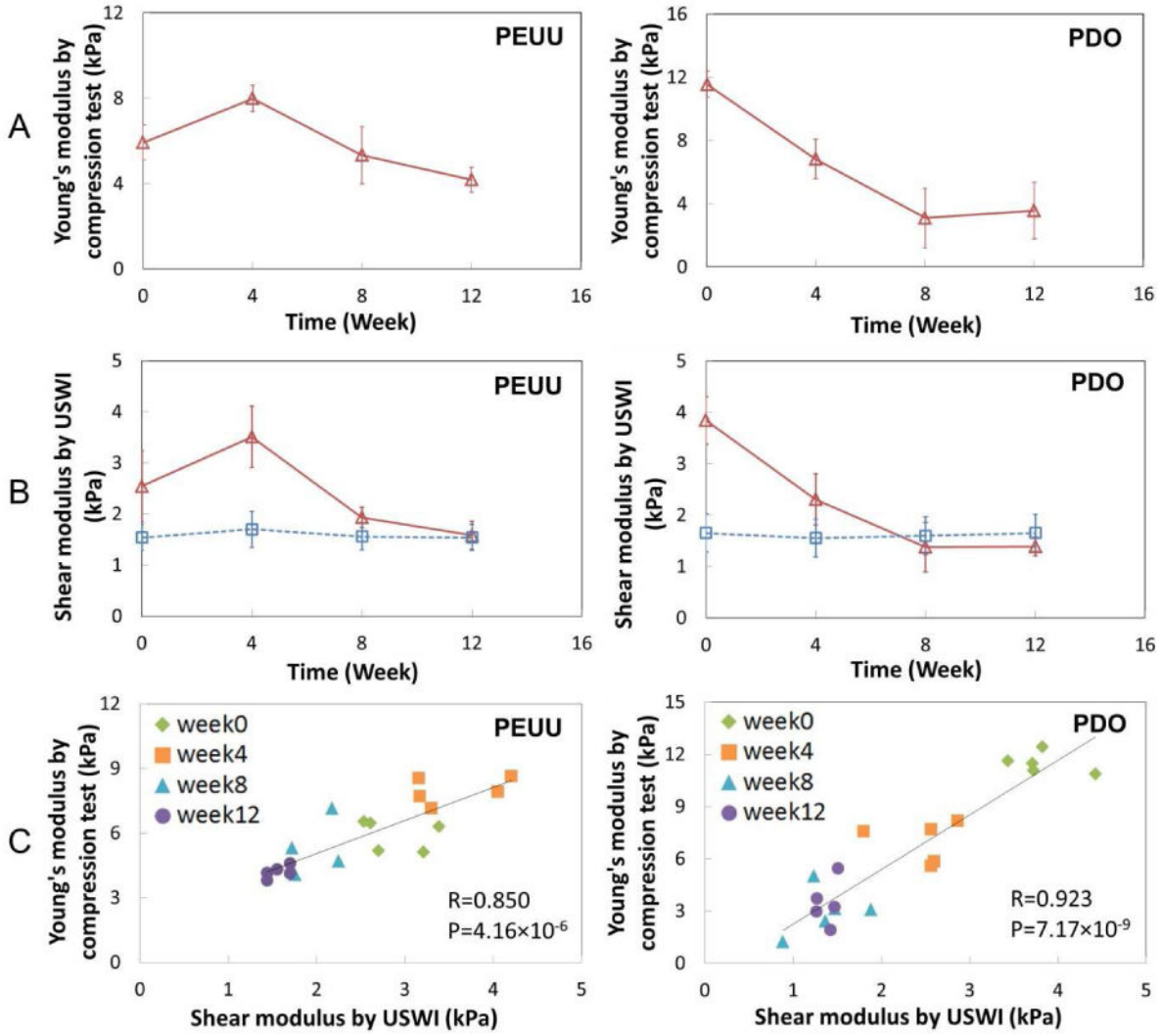

Fig. 4.

Comparison of elastic modulus obtained by USWI and direct compression measurements. (A) Young's modulus of PEUU and PDO constructs obtained by compression tests at weeks 0, 4, 8 and 12. Lines between two adjacent points are simple connection, not interpolation of data. (B) Average shear modulus of the constructs (red open triangle) and neighboring native abdominal wall tissues (blue open square) obtained by USWI over time. (C) Scatter plots of the Young's modulus and shear modulus from the same samples at corresponding time points. R denotes the correlation coefficient and P represents the p-value for the correlation between the Young's modulus (A) and shear modulus (B).

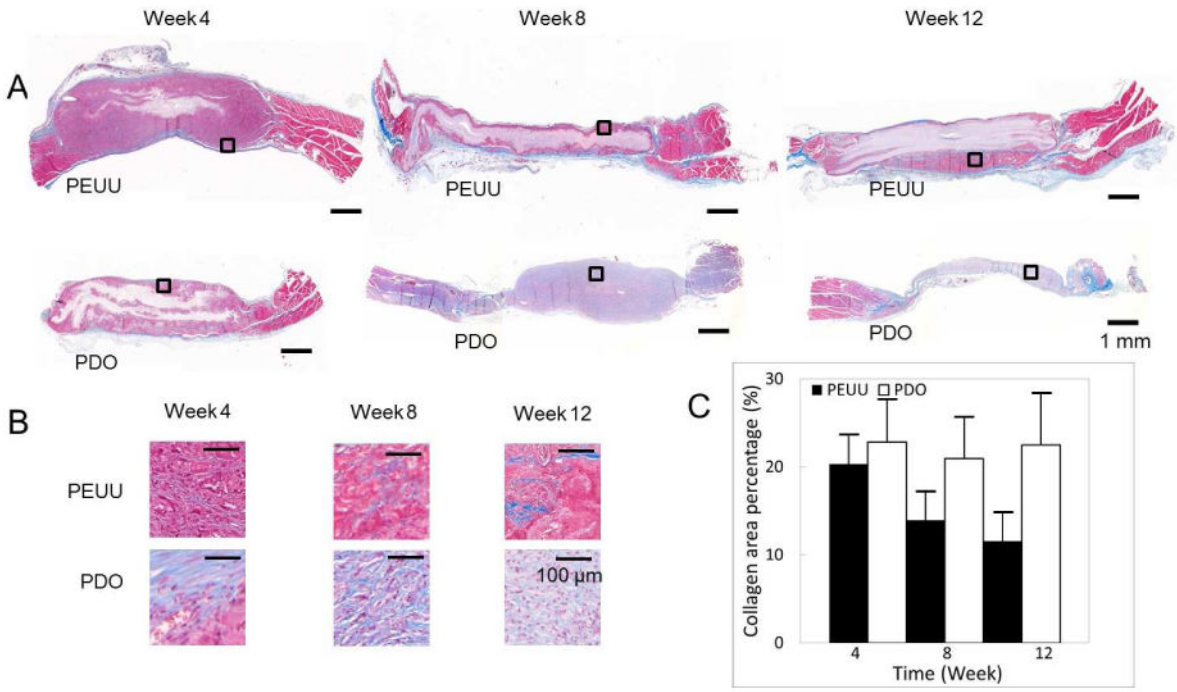

Fig. 5.

Histology. (A) Masson's trichrome (MT) stains for PEUU and PDO constructs at weeks 4, 8 and 12. (B) Representative magnified images taken from the selected area in the box in Fig. 4A. (C) Mean percent area of collagen deposition in the scaffolds as quantified from stained sections. (+ standard deviation)

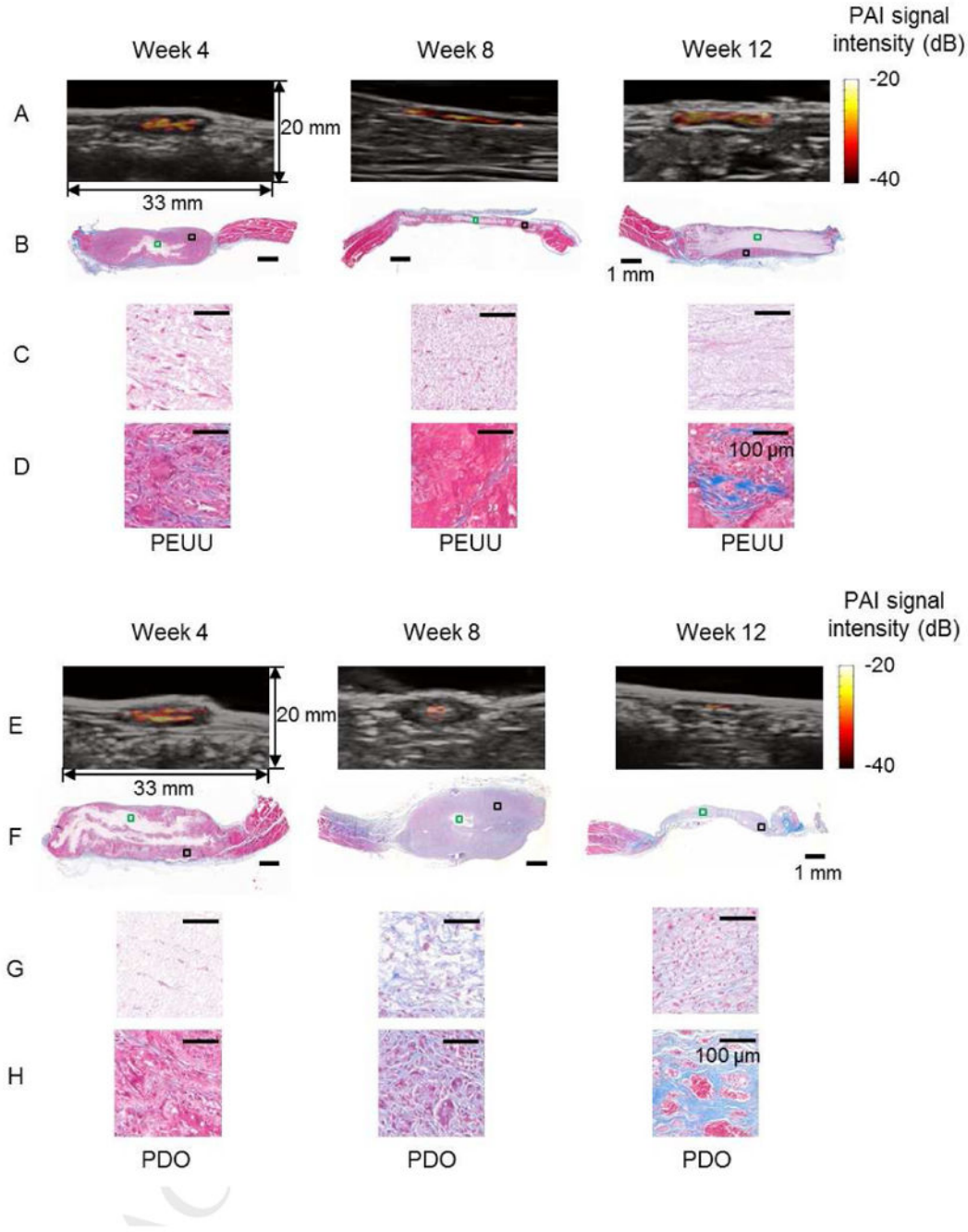

Fig. 6.

PAI of PEUU and PDO constructs. PAI maps and overlaid B-mode images for the PEUU (A) and PDO (E) constructs in the rat abdomen at weeks 4, 8 and 12. Masson's trichrome (MT) staining of PEUU (B) and PDO (F) constructs. Magnified images of representative areas (green box) in the central region of PEUU (C) and PDO (G) constructs. Magnified images of representative areas (black box) in the peripheral regions of PEUU (D) and PDO (H) constructs.

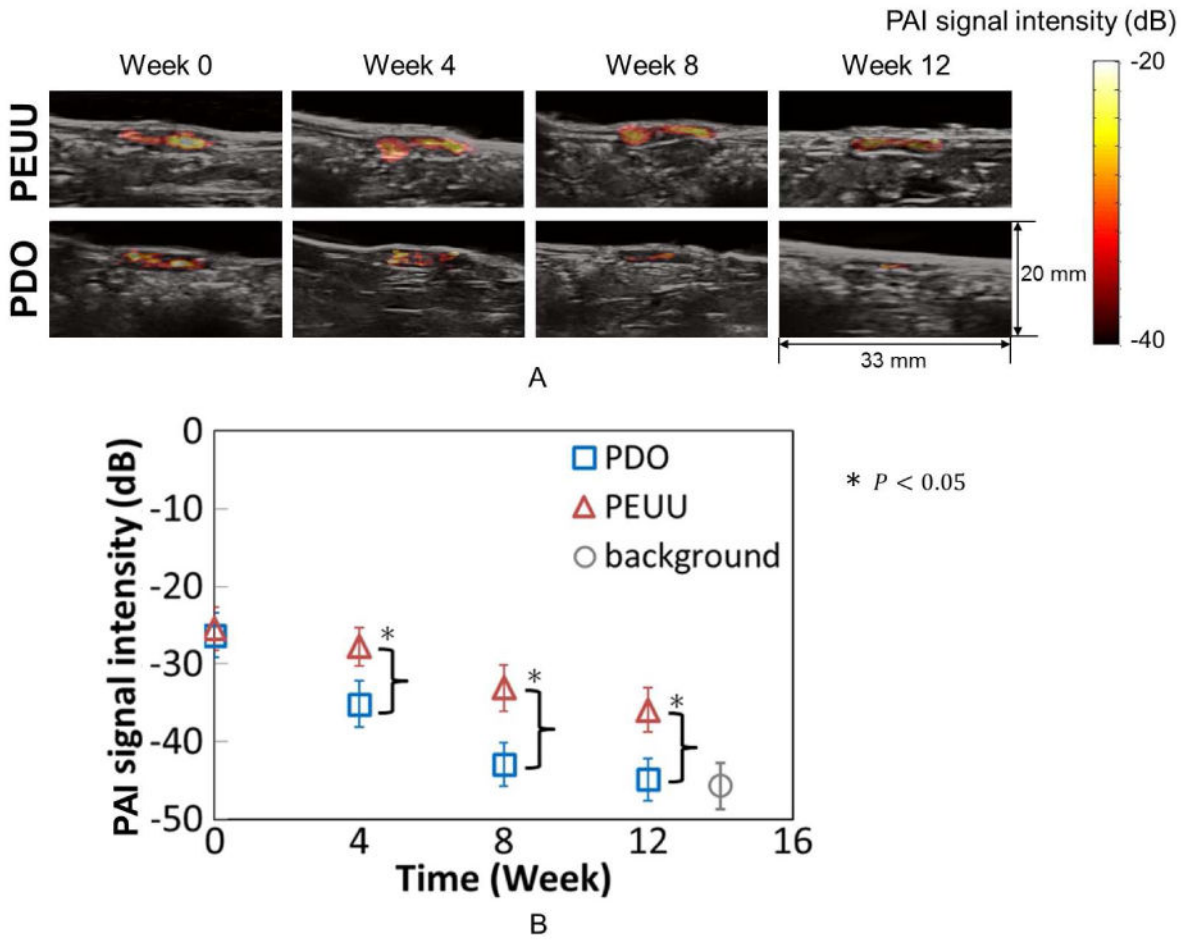

Fig. 7.

Longitudinal monitoring of structural changes of constructs by PAI. (A) PAI intensity map overlaid in the B-mode images for a rat implanted with PEUU (top panels) constructs and a rat implanted with PDO (bottom panels) constructs at weeks 0, 4, 8 and 12. Areas with high PAI signal intensity correspond to regions of remaining scaffolds with minimal tissue infiltration. (B) Average of PAI signal intensity of PEUU and PDO constructs at each time point. The background PAI signal intensity in Fig. 6B was obtained from the neighboring region to determine the baseline PAI signal intensity from tissues without scaffolds.

Biomaterials. Author manuscript; available in PMC 2015 September 01.

Table 1

Study design

Type of Scaffold	Weeks	Animals* sacrificed	Samples studied for USWI, PAI, and UEI	Samples for compression tests	Samples for histology
PEUU	0	3	10 (of 36)	6	0
	4	5	10 (of 30)	5	5
	8	4	10 (of 18)	4	4
	12	5	10 (of 10)	5	5
PDO	0	3	10 (of 36)	6	0
	4	5	10 (of 30)	5	5
	8	5	10 (of 20)	5	5
	12	5	10 (of 10)	5	5

*All animals were scanned before sacrifice